

Impacts of Saharan dust and clouds on photosynthetically available radiation in the area off Northwest Africa

By THOMAS OHDE* and HERBERT SIEGEL, *Leibniz Institute for Baltic Sea Research, Seestraße 15, DE 18119, Warnemünde, Germany*

(Manuscript received 22 September 2011; in final form 19 December 2011)

ABSTRACT

Radiation measurements in the area off Northwest Africa (research cruise, February 2008) and at Mindelo (Cape Verde Islands, May 2009) were used to investigate the impacts of Saharan dust and clouds on solar irradiance and on photosynthetically available radiation, to derive a relationship between dust aerosol optical depth (AOD) and photosynthetically available radiation and to determine the annual variations of photosynthetically available radiation. Three different kinds of atmospheric conditions were considered: cloudy skies, which decreased or increased the irradiance and dusty skies. The reduction by clouds was up to 67.2% at 400 nm and up to 84.4% at 700 nm. Enhancements of up to 21.9% at 400 nm and 34.0% at 700 nm were observed. The decrease by dust was up to 19.7% at 400 nm and up to 4.1% at 700 nm. Clouds decreased or increased the photosynthetically available radiation by up to 79.9% or up to 31.2%. The reduction by dust depended on the dust AOD and was between 3.6% and 12.3%. A linear relationship confirmed a decrease of photosynthetically available radiation of 1.2% by an increase of dust AOD of 0.1.

Keywords: Saharan dust, downward solar irradiance, photosynthetically available radiation, Northwest Africa

1. Introduction

The present study investigated the influence of Saharan dust on downward solar irradiance and photosynthetically available radiation on the basis of irradiance measurements at sea level within the framework of the German project, Surface Ocean Processes in the Anthropocene (SOPRAN), as part of the international study, Surface Ocean – Lower Atmosphere Study (SOLAS). The primary objective of SOLAS is the understanding of the biogeochemical-physical interactions and feedbacks between the ocean and the atmosphere. Several other projects investigated the dust effects in the atmosphere, the dust production and transport as well as the dust removal. Especially, strong efforts were undertaken in the area of western Africa and the tropical Atlantic to characterise the optical properties of desert dust particles, their radiative effects and their impact on weather and climate. The Saharan Dust Experiment investigated the transport to the tropical Atlantic (Tanré et al., 2003). The Dust and Biomass-burning

Experiment and the National Aeronautics and Space Administration – African Monsoon Multidisciplinary Analysis (NASA – AMMA) campaign studied the aerosol properties and their relations to the climate (Haywood et al., 2008; Chen et al., 2010). The Saharan Mineral Dust Experiment (SAMUM-1/SAMUM-2) investigated among others, the chemical composition, the size distribution and the optical properties of dust (e.g. Ansmann et al., 2011; Weinzierl et al., 2011; Lieke et al., 2011).

Our paper covered only one aspect of the German SOPRAN sub-project: ‘Sahara dust impact on radiation transfer, optical properties and phytoplankton development in waters of the Cape Verde region’, namely the interactions between dust and downward solar irradiance as well as dust and photosynthetically available radiation. The downward irradiance (units of $\text{mW m}^{-2} \text{nm}^{-1}$) is defined as the cosine-weighted radiance in relation to the angle of incident radiation integrated over the upper hemisphere (e.g. Jerlov, 1976; Morel and Smith, 1982). The photosynthetically available radiation (units of $\mu\text{mol m}^{-2} \text{s}^{-1}$) is the flux of quanta in the visible spectral range and represents the light available to photosynthetic processes. This quantity is defined as the integral over the

*Corresponding author.
email: thomas.ohde@io-warnemuende.de

previously defined downward irradiance weighted with the wavelength and integrated from 400 to 700 nm (e.g. Kirk, 1977; Gregg and Carder, 1990). The photosynthetically available radiation is directly related to the phytoplankton growth and compositions because of their photolimitation and photoinhibition properties (e.g. Dickey and Simpson, 1983; Arnone, 1994; Arnone et al., 1998).

Atmospheric dust and clouds affect the solar radiative transfer by absorption, scattering or reflection. The incident energy flux is influenced (e.g. Carlson and Benjamin, 1980; Stephens and Tsay, 1990), the spectral distribution of the radiation is modified (Frederick and Erlick, 1997; Haywood et al., 2003) and the solar energy available to photosynthesis is changed (Bartlett et al., 1998; Frouin and Murakami, 2007).

The modifications of spectral energy distribution by dust in the atmosphere impact light-dependent biological processes like phytoplankton growth in the euphotic zone of the oceans (Claustre et al., 2002; Wozniak and Stramski, 2004; Stramska et al., 2008). Even the composition and evolution of marine ecosystems can be regulated by such environmental conditions (Wiggert and Murtugudde, 2007; Mallet et al., 2009).

In addition to the effect of dust, the downward solar irradiance and consequently the photosynthetically available radiation are influenced by cloudiness. Usually clouds attenuate the downward solar irradiance depending on the type of clouds. The solar radiation under cirrus clouds can be 70% compared to clear sky. A deep layer of stratus clouds may transmit only 10% of the solar radiation (Monteith, 1973). However, in contrast to the attenuation, isolated white cumulus clouds at an otherwise clear sky, which do not obscure the sun, can increase the downward solar irradiance by increase of the diffuse sky radiation (Kirk, 1994).

The amount and the type of clouds determine the amount of photosynthetically active radiation. Reductions of about 35%, 30% and 10% were observed for low-, medium- and high-level clouds with fractional cloud coverage of nearly one (Alados et al., 2000). Kasten and Czeplak (1980) as well as Davies (1995) determined a decrease of up to 45% compared to clear sky. The spectral modifications of the incident solar radiation by clouds also effect the photosynthetically active radiation. The spectral effect of clouds caused a reduction of about 4% (Bartlett et al., 1998). Only some papers about the interactions between dust and photosynthetically active radiation in the desert areas of China and Nigeria were published. The measurements established that the photosynthetically active radiation of dust days was obviously smaller than for clear days (Udo and Aro, 1999; Jimin et al., 2006).

One aim of the paper was the quantification of the spectral modification in the study area off Northwest (NW)

Africa. Another goal was the determination of the reduction of photosynthetically available radiation by dust storms in comparison to the impact of clouds. The overall objective was the determination of the annual variations of photosynthetically available radiation due to atmospheric dust.

The paper is structured as follows: First, the applied method and the study area are briefly introduced in Sections 2.1 and 2.2. An overview of used data sets and data processing is given in Section 2.3 and in Sections 2.4.1 to 2.4.5. Section 2.4.6 is dedicated to the description of an approach for the comparison of irradiance measurements during different times, locations and atmospheric conditions. This approach is used to investigate the modifications of irradiance and photosynthetically available radiation caused by atmospheric dust and different kinds of clouds (Section 3).

2. Methodology

2.1. Method

The measured irradiances at sea level were related to the atmospheric conditions during the measurements using different data sets (see Sections 2.3–2.4). Days with clear sky, with Saharan dust events and with different cloud conditions were identified by analysis of the irradiance spectra, by comparison to the dust component of aerosol optical depth (AOD) and by correlations to modelled irradiances (see Sections 3.1 and 3.2). In order to compare irradiance measurements for different days and conditions, they were normalised to the same zenith angle, geographical location and atmospheric conditions on the basis of a spectral solar irradiance model (see Section 3.3). The influence of dust and clouds on photosynthetically available radiation derived from spectral irradiance measurements was investigated in Section 3.4. The effect of dust was quantified in comparison to cloudy and clear sky observations (see Section 3.4). The variations of photosynthetically available radiation caused by atmospheric dust were used to derive a relationship between the dust component of AOD and the photosynthetically available radiation. This relation was applied to describe the annual variations in photosynthetically available radiation in the study area off NW Africa (see Section 3.4).

2.2. Study area

The study area was located off NW Africa with a longitudinal extent of 16° W to 25° W and a latitudinal extent of 15° N to 20° N (Fig. 1). This area is well-known for Saharan dust storms (e.g. Prospero and Carlson, 1972; Kalu, 1979; Chiapello and Moulin, 2002). The dust transport is strongly variable and depends on the season

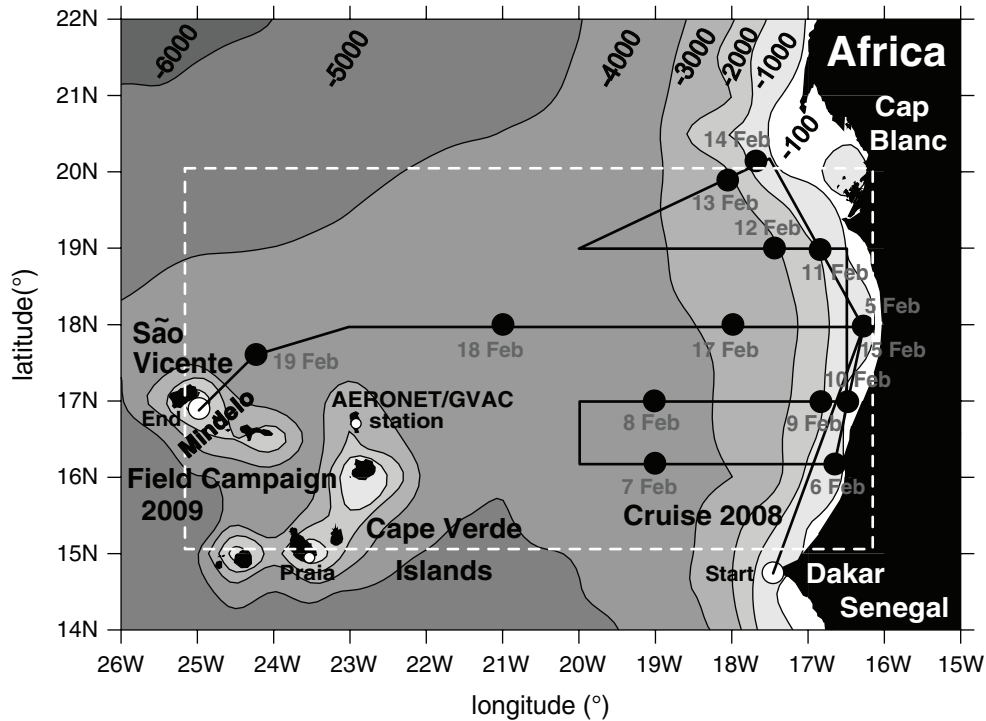


Fig. 1. The study area was located between Dakar, Cap Blanc and the Cape Verde Islands covered by the white-dashed box between 16° W and 25° W and 15° N and 20° N. The map shows the ship track (black line from point ‘Start’ to point ‘End’; black points correspond to the position of the ship: e.g. 5 Feb = 5 February 2008) of the first cruise from 5 to 19 February 2008 and the location of the permanent station in Mindelo on the island São Vicente of the second field campaign from 19 to 28 May 2009. The statistics of dust storms of 2008 to 2009 were determined from daily dust aerosol data, which were area-averaged for the white-dashed box. The location of the AERONET station and the METAR station GVAC on the Cape Verde Island Sal is included.

(Kaufman et al., 2005). Dust of nearly 1.4×10^{11} kg is transported to the tropical North Atlantic Ocean during boreal summer (e.g. Prospero et al., 1981; Prospero and Lamb, 2003). The dust storms in winter and spring are related to intense westward winds, which transport the dust material to the Cape Verde region (e.g. Schepanski et al., 2009). High variability of atmospheric layers in the Cape Verde region was established by meteorological, lidar, particle and radiation measurements at the airport Praia (Fig. 1) and with the Deutsches Zentrum für Luft- und Raumfahrt Falcon research aircraft during the SAMUM project (e.g. Ansmann et al., 2011; Knippertz et al., 2011; Petzold et al., 2011; Toledano et al., 2011; Weinzierl et al., 2011). Different aerosol layers were found in January and February 2008: maritime layers (M), pure dust layers (D), biomass-burning layers (BB), mixtures of dust and maritime aerosols (D/M) but also mixtures of dust and biomass-burning layers (D/BB). Various complex stratifications of these layers were experimentally verified: M + D + D/BB, D + D/BB, pure dust or pure maritime layers in the lower atmosphere without BB layers aloft, M + D/BB or D + BB (Knippertz et al., 2011, Weinzierl

et al., 2011). The aerosol types and their mixing and layering in the Cape Verde region depend mainly on the meteorological conditions (e.g. Schepanski et al., 2009), the fire activities in southern West Africa (Barbosa et al., 1999; Haywood et al., 2008) and the export of Saharan dust from arid African regions (e.g. Goudie and Middleton, 2001).

2.3. Data basis

2.3.1. Downward solar irradiance at sea level. The wavelength (λ) dependent spectral downward (subscript d) solar irradiance $E_d(\lambda)$ was measured in units of $\text{mW m}^{-2} \text{nm}^{-1}$ at sea level (just above the water surface) during two field campaigns [notations of Gordon et al. (1983) as well as Gregg and Carder (1990) were used].

The first cruise on board of R.V. ‘L’Atalante’ started in Dakar (Senegal) on 5 February 2008 and ended in Mindelo (Cape Verde) on 19 February 2008. The downward solar irradiance was measured with a time resolution of 30 s during the whole cruise (black line in Fig. 1). The irradiance sensor was mounted at the bow of the research

vessel. The zenith alignment of the sensor varied between 0 and 5 deg because of the ship's movement.

During the second field campaign, the measurements were performed between 19 and 28 May 2009 (Fig. 1) with the same temporal resolution (30 s) in Mindelo (16.87° N, 24.98° W) on the island São Vicente. The irradiance sensor was mounted on top of a near coastal building in Mindelo and was directed to the zenith.

RAMSES-ACC-VIS hyperspectral radiometer manufactured by TriOS (Oldenburg, Germany) was used for irradiance measurements. The radiometer had 190 usable channels covering the wavelength range from 320 to 950 nm with a spectral sampling of 3.3 nm per pixel. The built-in miniature spectrometer was produced by Carl ZEISS (Jena, Germany) and consisted of a quartz fibre bundle, which ended in the slit of the spectrograph (Heuermann et al., 1999). The detector type was a silicon photodiode array. The cosine collector consisted of a diffusing glass, and the integration time was automatically adjusted. The calibration was made by the manufacturer in November 2007 using a calibrated tungsten lamp for the visible part of the light spectrum, which was driven by stabilised power supplies (NIST standard). The spectral accuracy of the spectral calibration was 0.3 nm. Detailed descriptions of the hyperspectral radiometer and the field calibrator were given in the manuals of the manufacturer (<http://www.trios.de>).

The uncertainty of the downward solar irradiance measurements consisted of uncertainties from RAMSES-ACC-VIS instrument and from misalignments of the radiometer. The instrumental uncertainties were between 6% and 10% depending on the spectral range (Heuermann et al., 1999). The misalignments produced by the ship movements were estimated by the approach of Seckmeyer et al. (2005) and Wuttke et al. (2007). The irradiance deviations from a perfectly aligned zenith instrument were smaller than 2% during our research cruise.

2.3.2. Aerosol optical depth

2.3.2.1. Satellite AOD: Space-borne AOD measurements by Moderate Resolution Imaging Spectroradiometer (MODIS) onboard the satellites Aqua and Terra were used to approximate the optical depth of the dust component during the two field campaigns in the study area (Fig. 1) and by that to classify the observed dust storms in relation to their strength.

Daily data of total AOD at 550 nm and fine mode fraction (f) in a horizontal resolution of 1 deg \times 1 deg were downloaded from the Giovanni archive (<http://daac.gsfc.nasa.gov>). This archive provided the Aqua and Terra level 2 products MOD08_D3.051 and MYD08_D3.051 in the processing version 5.1. The AOD product is the measure of radiation attenuation due to atmospheric aerosol scattering

and absorption. The value f is the ratio of the fine mode of AOD (AOD_{fine}) to AOD at 550 nm. The AOD is derived with an error of ± 0.03 (Tanré et al., 1997), and the uncertainty of f is ± 0.2 (Tanré et al., 1996, 1997). The MODIS products of AOD and AOD_{fine} were explained in detail in the MODIS Algorithm Theoretical Basis Documents (<http://modis.gsfc.nasa.gov>). Both quantities were used to separate the different aerosol components (maritime, dust, anthropogenic) according to the method of Kaufman et al. (2005) (see Section 2.4.2). The sources of maritime and dust aerosols were the sea-spray emissions in the Atlantic Ocean and the dust production in arid regions of Africa, respectively (e.g. Goudie and Middleton, 2001). The anthropogenic aerosol component came from the smoke of biomass-burning activities in southern West Africa (e.g. Weinzierl et al., 2011). The mixing, layering and stratification of different aerosol types in the area of Cape Verde Islands was very complex and highly variable (e.g. Ansmann et al., 2011; Knippertz et al., 2011). Therefore, the separation approach of Kaufman et al. (2005) was only an approximation for the atmospheric aerosol content during our observation periods. The uncertainties for the maritime and dust aerosol components were about 10% and 10%–15%, respectively (Kaufman et al., 2005). The error in the anthropogenic part was assumed in the same order.

2.3.2.2. Ground-based AOD: Ground-based AOD data were used to evaluate the MODIS-derived AODs and to eliminate outliers in the MODIS data set.

The cloud-screened and quality-assured level-2 total aerosol data at 440 nm and 675 nm (AOD_{AERONET}) derived from automated CIMEL sunphotometers of February 2008 and May 2009 were downloaded from the Aerosol Robotic Network (AERONET, aeronet.gsfc.nasa.gov). The AOD_{AERONET} data of the AERONET station ('Capo_Verde', 16.73° N and 22.93° W, see Fig. 1) nearest to our study area were used. The level-2 data were pre- and post-field calibrated, automatically cloud cleared and manually inspected (e.g. Tanré et al., 1997, 2003). The AERONET aerosol data at 440 nm and 675 nm were the basis for the determination of AOD_{AERONET} at 550 nm (see Section 2.4.2).

Typically, the absolute total uncertainty in AOD from a newly calibrated field instrument under cloud-free conditions is smaller than 0.02 (Holben et al., 1998).

2.3.3. Meteorological data. Meteorological data were used to estimate the contribution of dust to the total AOD, to normalise the downward solar irradiance, and they were taken as input for the irradiance model.

The atmospheric sea level pressure P and the relative humidity RH of National Centers for Environmental Prediction (NCEP) reanalysis 2 data set were downloaded (<ftp://ftp.cdc.noaa.gov>) in a spatial and temporal resolution of about 2 deg and 6 h (Kalnay et al., 1996; Kanamitsu et al., 2002). Quick Scatterometer (QuikScat) and Advanced Microwave Scanning Radiometer (AMSR-E) daily wind speeds W with a spatial resolution of 0.25 deg were obtained from the Remote Sensing System, Santa Rosa (<http://www.remss.com>) (Ebuchi et al., 2002, 2006; Bourassa et al., 2003; Chelton and Freilich, 2005). The AMSR-E measurements of total precipitable water WV in a resolution of 0.25 deg were also taken from Remote Sensing System. The total ozone data (O_3) were extracted from the Meteosat Second Generation (MSG) product (Drouin and Karcher, 2004), which was downloaded from the European Organisation for the Exploitation of Meteorological Satellites (EUMETSAT) archive (<http://archive.eumetsat.int>). The visibility V was taken from meteorological observations (METAR reports) at Sal, Cape Verde (Fig. 1), provided by National Center for Atmospheric Research/Earth Observation Laboratory (NCAR/EOL) under sponsorship of the National Science Foundation (NSF). The METAR data were collected by the University Corporation of Atmospheric Research/Joint Office of Science Support (UCAR/JOSS; <http://data.eol.ucar.edu>).

2.4. Data processing and methodological aspects

2.4.1. Downward solar irradiance. The raw measurements of RAMSES-ACC-VIS hyperspectral radiometer were converted with current calibration files of November 2007 to downward solar irradiance values $E_d(\lambda)$ on the basis of the standard TriOS software MSDA_XE. During the field measurements in February 2008 and May 2009, the irradiance sensors were controlled before and after each campaign by a field calibrator FieldCAL (TriOS, Oldenburg, Germany). The stability of the radiometer throughout the experiments was very good. The deviations were below 1% compared to the calibration made by the manufacturer.

2.4.2. Aerosol optical depth. The following processing steps were carried out to generate area-averaged aerosol components for the identification, characterisation and statistics of dust storms in the study area:

- (1) The maritime (sea salt), soil (dust) and anthropogenic (smoke from biomass-burning, industrial pollution) components of the AOD (AOD_{ma} , AOD_{dust} and AOD_{an}) at 550 nm were derived from daily MODIS AOD data and fine mode fraction f , according to the method of Kaufman et al. (2005).

Only high-quality MODIS data were used. The maritime component of AOD was calculated using the wind speed of QuikScat. The AOD_{dust} error was 10–15% for $AOD_{dust} > 0.1$ (Remer et al., 2002; Kaufman et al., 2005).

- (2) The aerosol components (maritime, dust and anthropogenic) were averaged over a 1 deg \times 1 deg box along the ship track during the cruise in February 2008. For the field campaign in May 2009 the box was permanently centred on the land station Mindelo. The area-averaged approach was used because the ship positions and the permanent position of the land station were not located in the centre of 1 deg \times 1 deg source boxes delivered by Giovanni archive. Therefore, the surrounding boxes were taken into account. Within this method, the daily aerosol components AOD_{ma} , AOD_{dust} and AOD_{an} were area-averaged according to $\bar{x}_t = \frac{1}{N} \sum_{i=1}^N \bar{x}_{t,i}$, where \bar{x}_t was the area-averaged component at time step t , $\bar{x}_{t,i}$ were the data values at time step t that lay in the chosen latitude and longitude range and N was the corresponding number of data points in that geographical grid. Area-averaged aerosol data were used to minimise statistical errors caused by data gaps, clouds contaminations and different satellite swaths.
- (3) The procedure of area-averaging described in point 2 was also applied to the white-dashed box (see Fig. 1) for statistical considerations in relation to dust storms of 2008 and 2009. The box was defined to cover the study area and the stations of both field campaigns. This approach delivered mean values of area-averaged components of AOD, their standard deviations, the number of strong dust storms, the mean duration times of strong dust events and their standard deviations.
- (4) The AERONET data (Section 2.3.2.2) were used for the derivation of $AOD_{AERONET}(550 \text{ nm})$, for comparison with MODIS aerosol data and for elimination of outliers in the MODIS data set. The AERONET data sets could not be applied for the derivation of aerosol components because the decomposition was based on MODIS derived aerosol optical depth (Kaufman et al., 2005). The Ångström exponent α , a measure of the aerosol size distribution, was determined by a log-linear fit using the relation $\ln AOD_{AERONET} = -\alpha \ln \lambda + \ln \beta$ on the basis of the AERONET data at two wavelengths, i.e. $\lambda = 440 \text{ nm}$ and $\lambda = 675 \text{ nm}$. The approximated AODs at 550 nm were computed from Ångström power law $AOD_{AERONET} = \beta \lambda^{-\alpha}$ where β was the Ångström's turbidity exponent. In this approximation it was assumed that both parameters

α and β were independent to the wavelength. Newest measurements of AOD of pure atmospheric dust layers established deviations from the Ångström power law, mainly in the ultraviolet and infrared (Toledano et al., 2011). The deviations of the linear fit to the new third-order polynomial fit were only in the order of few percent in the wavelength range 440–675 nm (see Fig. 6b in Toledano et al. (2011)). The AOD data at 550 nm of AERONET and MODIS data sets were fitted with linear regression, where N is the number of data points, R^2 is the coefficient of determination and S is the slope of the linear fit. For the cruise in February 2008 was found $N=18$, $R^2=0.95$ and $S=1.57$ were found, and for the field campaign in May 2009 was determined $N=12$, $R^2=0.93$ and $S=0.94$ were determined. Outliers in the MODIS data set were identified by strong deviations from the regression line.

2.4.3. Statistics of dust storms. All dust storms in the years 2008 and 2009 were identified on the basis of area-averaged dust AODs using the separation approach of Kaufman et al. (2005) (cf. Section 2.4.2). The goal was a strength classification of the observed dust storms of the field campaigns in February 2008 and May 2009 (cf. results in Section 3) and the derivation of a dust storm statistics of both years.

The mean value of area-averaged dust component of AOD $\langle \text{AOD}_{\text{dust}} \rangle$ and the corresponding standard deviation σ of the investigation period of 2008–2009 were determined to 0.37 and 0.35 (cf. Section 2.4.2). Strong events were defined by the limit $\langle \text{AOD}_{\text{dust}} \rangle + \sigma = 0.72$. All AOD_{dust} values greater than this value belonged to strong dust storms. During the study period, 29 strong individual dust storms with a mean duration of 2.7 d and a standard deviation of 1.6 d were observed. Dust storms below the defined limit were classified as moderate dust events, but AOD_{dust} values smaller than $\langle \text{AOD}_{\text{dust}} \rangle - \sigma = 0.02$ were characterised as atmospheric conditions with nearly no dust in the atmosphere. The dust storm with the highest dust component of AOD of 2.64 was observed on 17 July 2008.

2.4.4. Meteorological data. The temporal and spatial resolutions of meteorological data like P , RH , W , WV , O_3 and V were different depending on the method of their measurement. Therefore, all meteorological data were processed to derive a common data basis with same temporal and spatial resolutions. The first processing step was the derivation of daily means. Then, all daily means were area-averaged with the same procedure used for aerosol data (cf. Section 2.4.2).

2.4.5. Cases of cloud impact on downward solar irradiance.

Two cases were defined according to the cloud influence on downward solar irradiance. All cloud conditions reducing the solar irradiance compared to cloudless sun and sky were summarised in the group ‘case I’. For instance, thin sheet of cirrus clouds, diffuse clouds, hazy atmospheric conditions or deep layers of stratus clouds belong to case I.

Mainly isolated cumulus clouds beside cloudless sun can enhance the downward solar irradiance by increase of the diffuse part of solar radiation. Such cloud conditions were divided in the ‘case II’ group.

The irradiance spectra of cloud conditions of case I and II were identified by analysis of all irradiance measurements of both field campaigns. They were found by comparison to clear sky measurements (see Section 3.2) and modelled clear sky irradiances (see Section 2.4.6). Irradiance peaks below the measured or modelled clear sky irradiance were identified as clouds of case I, and peaks above were considered as clouds of case II (see details in Section 3.2).

2.4.6. Irradiance normalisation, spectral model and photosynthetically available radiation.

The investigation of the spectral influence of dust and clouds on the incident irradiance required the comparison of irradiance measurements observed at different days and locations. It means that the conditions during the measurements could be varied due to different zenith angles θ (*time, location*), extraterrestrial irradiances F_o (*solar cycle, sun-earth distance*) and atmospheric conditions (P , RH , WV , V , ... see Section 2.3.3). Ideally, the dust (E_d^{sample} , *sample = dust*) or cloud observations (E_d^{sample} , *sample = cloud*) could be directly related to reference irradiance measurements ($E_d^{\text{reference}}$, *reference = clear sky, cloudless and dustless atmospheres*) at same conditions during the measurements (same zenith angle, same extraterrestrial irradiance, same atmospheric conditions like P , RH , WV , V , ... see Section 2.3.3). The wavelength-dependent irradiance differences between dust and dust- and cloudless atmosphere, cloud and cloud- and dustless atmosphere or mixed types would directly deliver the irradiance modifications by dust and clouds. However, the ideal case was not valid for the observed irradiances because the conditions were different between the measurements:

- (1) The zenith angles between sample and reference measurement varied with time and location of observations.
- (2) The extraterrestrial irradiance reaching the earth varied in dependence of solar cycle and sun–earth distance. Willson and Mordvinov (2003) derived the fluctuation of solar cycles of about 5 Wm^{-2}

per 20 yr by satellite measured extraterrestrial irradiance. This effect was neglected within the frame of the comparison of the irradiance measurements during both field campaigns of 2008 and 2009 because the relative error was smaller than 0.4% ($5 \text{ Wm}^{-2}/1367 \text{ Wm}^{-2} * 100\%$, where 1367 Wm^{-2} corresponds to the solar constant). In contrast, the different sun–earth distances during the different field measurements cannot be neglected because the maximum relative error would be 5.5% $\{[F_o(05 \text{ February } 2008)-F_o(28 \text{ May } 2009)]/F_o(28 \text{ February } 2008) * 100\%$.

- (3) The atmospheric conditions like atmospheric sea level pressure P , relative humidity RH , total precipitable water WV , visibility V and others (see Section 2.3.3) varied in the observation periods. The relative errors in relation to the different atmospheric conditions were much higher than the sun–earth distance error and cannot be neglected in our approach. All three points (1–3) must be considered by a correction term.

Therefore, dust and cloud observations were compared with reference irradiance measurements during cloudless and dustless maritime atmospheres by derivation of the absolute and relative irradiance deviations

$$\Delta E_d = co * E_d^{\text{sample}} - E_d^{\text{reference}}, \text{ and} \quad (1)$$

$$\frac{\Delta E_d}{E_d^{\text{reference}}} = \frac{co * E_d^{\text{sample}} - E_d^{\text{reference}}}{E_d^{\text{reference}}} * 100\% \text{ with} \quad (2)$$

$$co = \frac{E_d^{r,\text{mod}}}{E_d^{s,\text{mod}}}. \quad (3)$$

The wavelength-dependent correction term co was introduced in order to compare different irradiance measurements observed at different conditions by normalisation of sample irradiance E_d^{sample} to the conditions of reference irradiance $E_d^{\text{reference}}$. Note that $E_d^{r,\text{mod}}$ and $E_d^{s,\text{mod}}$ in eq. (3) were determined for cloudless and dustless maritime atmospheres with a spectral solar irradiance model, which will be introduced later. Therefore, the quotient co of both quantities was no correction in relation to clouds and dust. The correction term is nearly one for all wavelengths in the case of similar sun–earth distances, zenith angles and atmospheric conditions of modelled reference and sample irradiance and is one for identical conditions. In this case, the absolute and relative irradiance deviations (1) and (2) are equal to zero if $E_d^{\text{sample}} = E_d^{\text{reference}}$.

Our approach (eqs. 1 and 2) describes the modifications of downward irradiance due to dust and clouds compared to clear sky and was the basis for the following investigations. It is of course possible to use a different approach where the clear sky spectra would be calculated by spectral

solar irradiance model and the differences $E_d^{\text{sample}}(\text{measured}) - E_d^{\text{reference}}(\text{calculated})$ would be determined without the correction term of eq. (3). This approach was not used because only differences (eqs. 1 and 2) of measurements should be determined. Furthermore, the model has to be adjusted precisely to avoid additional errors and should be trustworthy, as well as an instrumental correction factor has to be considered (Bartlett et al., 1998).

The modelled reference irradiance $E_d^{r,\text{mod}}$ and the modelled sample irradiance $E_d^{s,\text{mod}}$ of cloudless and dustless maritime atmospheres were calculated using the spectral solar irradiance model of Gregg and Carder (1990). This irradiance model provided downward irradiance from 400 to 700 nm with high spectral resolution of 1 nm. Processes like scattering and absorption by gas mixtures, absorption by ozone, scattering and absorption by maritime aerosols and absorption by water vapour were included. The downward irradiance was calculated by the sum of their direct (E_{dd}) and diffuse components (E_{ds})

$$E_{dd} = F_o T_r T_a T_{Oz} T_o T_w \cos \theta, \quad (4)$$

$$E_{ds} = I_r + I_a, \quad (5)$$

where T_r , T_a , T_{Oz} , T_o and T_w represented transmissivity after absorption or scattering by air molecules, aerosols, ozone, oxygen and water vapour, respectively (Bird and Riordan, 1986). The quantities I_r and I_a were the diffuse components due to Rayleigh and aerosol scattering. The direct component (eq. 4) and the diffuse component (eq. 5) were calculated according to Gregg and Carder (1990) with the meteorological data set given in Sections 2.3.3 and 2.4.4. The root mean square model error for the wavelength range from 400 to 700 nm was only 6.2% over all atmospheric conditions (Gregg and Carder, 1990).

The absolute and relative modifications of photosynthetically available radiation (Q_{PAR}) by dust storms and different clouds (case I and II) were investigated with

$$\Delta Q_{\text{PAR}} = Q_{\text{PAR,corr}}^{\text{sample}} - Q_{\text{PAR}}^{\text{reference}}, \text{ and} \quad (6)$$

$$\frac{\Delta Q_{\text{PAR}}}{Q_{\text{PAR}}^{\text{reference}}} = \frac{Q_{\text{PAR,corr}}^{\text{sample}} - Q_{\text{PAR}}^{\text{reference}}}{Q_{\text{PAR}}^{\text{reference}}} * 100\% \text{ with} \quad (7)$$

$$Q_{\text{PAR,corr}}^{\text{sample}} = \frac{1}{hc} \int_{400}^{700} \lambda * co * E_d^{\text{sample}} d\lambda \text{ and} \quad (8)$$

$$Q_{\text{PAR}}^{\text{reference}} = \frac{1}{hc} \int_{400}^{700} \lambda * E_d^{\text{reference}} d\lambda \quad (9)$$

where $Q_{\text{PAR,corr}}^{\text{sample}}$ was the corrected photosynthetically available radiation of the sample (*sample = dust or cloud*) and $Q_{\text{PAR}}^{\text{reference}}$ was the photosynthetically available radiation of reference during clear sky (*reference = clear sky*). The

quantity h was the Planck's constant and c was the velocity of light in vacuum. The variables E_d^{sample} and $E_d^{\text{reference}}$ corresponded to measurements of RAMSES-ACC-VIS hyperspectral radiometer. The integration limits were defined from 400 to 700 nm according to Gregg and Carder (1990).

The following processing steps were necessary to study the impact of clouds and dust on the incident irradiance and photosynthetically available radiation:

- The procedure started with the identification of measurements at different atmospheric conditions by the analysis of daily irradiance cycles. The Saharan dust observations were separated from other atmospheric conditions using dust AODs (see Sections 3.1 and 3.2). The irradiance measurements performed during clear sky were detected by comparison to modelled irradiances (see Section 3.2). Clouds were identified using their attenuation or enhancement of irradiances compared to clear sky measurements (see Sections 2.4.5 and 3.2).
- The measured irradiances during dust and cloud conditions were adjusted by the introduced correction term (eq. 3) to avoid differences in geometry due to sun zenith distance or location and in atmospheric conditions (see Sections 2.4.6 and 3.3).
- The final step was the investigation of the impact of dust on downward irradiance and photosynthetically available radiation in comparison to the influence by clouds (see Section 3.4).

3. Results and discussions

3.1. Classification and characterisation of observed dust storms

The area-averaged maritime, dust and anthropogenic components of the AOD (AOD_{ma} , AOD_{dust} , AOD_{an}) at 550 nm are presented in Fig. 2A and B, respectively, for the cruise in February 2008 (panel A) and for the field campaign in May 2009 (panel B). The ground-based total AOD of AERONET station at 550 nm (AOD_{AERONET}) was given for comparison.

Sahara dust storms were identified by analysis of AOD_{dust} and AOD_{AERONET} (Fig. 2A and B). High values were related to high atmospheric dust load. The dust events also corresponded to reduced measured irradiances (cf. with Fig. 3A and B) and were verified in quasi-true colour images of MODIS by their yellow discolouration (not shown).

Saharan dust storms were observed during both field campaigns. The first one was clearly determined between 16 and 19 February 2008, with maximum $AOD_{\text{dust}} = 0.92$ on

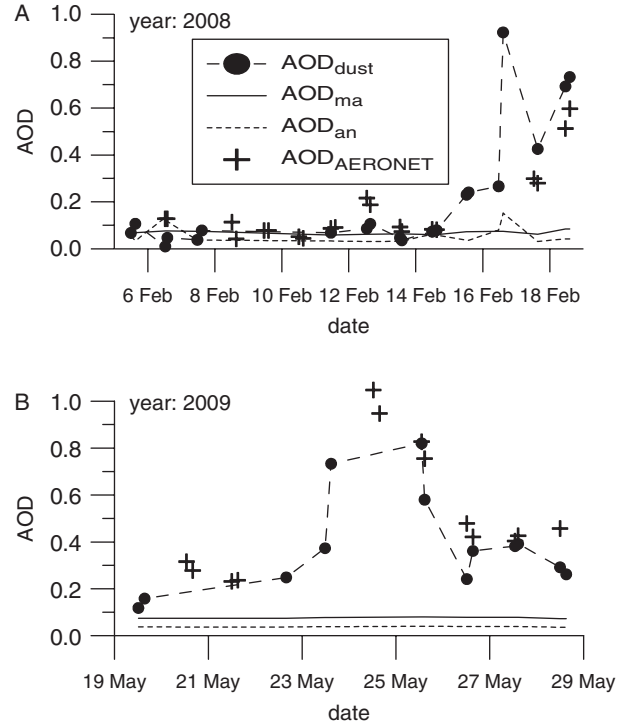


Fig. 2. The MODIS aerosol components AOD_{dust} , AOD_{ma} and AOD_{an} at 550 nm of cruise 2008 (panel A) and of field campaign 2009 (panel B) are shown. The dust storms are clearly seen between 16 and 19 February 2008 as well as between end of 23 May and 27 May 2009. The total aerosol optical depth of AERONET station (AOD_{AERONET}) at 550 nm is given for comparison.

16 February 2008. The second dust storm was observed between 23 May and 27 May 2009 with values of AOD_{dust} around 0.82 on 25 May 2009, but AOD_{AERONET} indicated a maximum on 24 May 2009 of about 1.00 (cf. AOD_{AERONET} data in panel B of Fig. 2). Both dust storms belonged to strong storms because their maximum values exceed the defined limit of 0.72 (see Section 2.4.3). The dust storm in February lasted about 3 d with a peaked maximum and the storm in May about 4 d with a broader maximum. The storms were longer than the statistically determined mean duration of 2.7 d.

The maritime and anthropogenic components of the AOD (AOD_{ma} and AOD_{an}) were nearly constant. Mean values of 0.07 and 0.05 in February 2008 and of 0.08 and 0.04 in May 2009 were derived, implying that the variability of total AOD was mainly caused by the dust component. The aerosol components were determined with uncertainties (see Section 2.3.2.1) because of the separation approach of Kaufman et al. (2005), which could not fully describe the variability of aerosol layers and their very complex stratification (e.g. Ansmann et al., 2011; Weinzierl et al., 2011). Different layer structures were observed during the

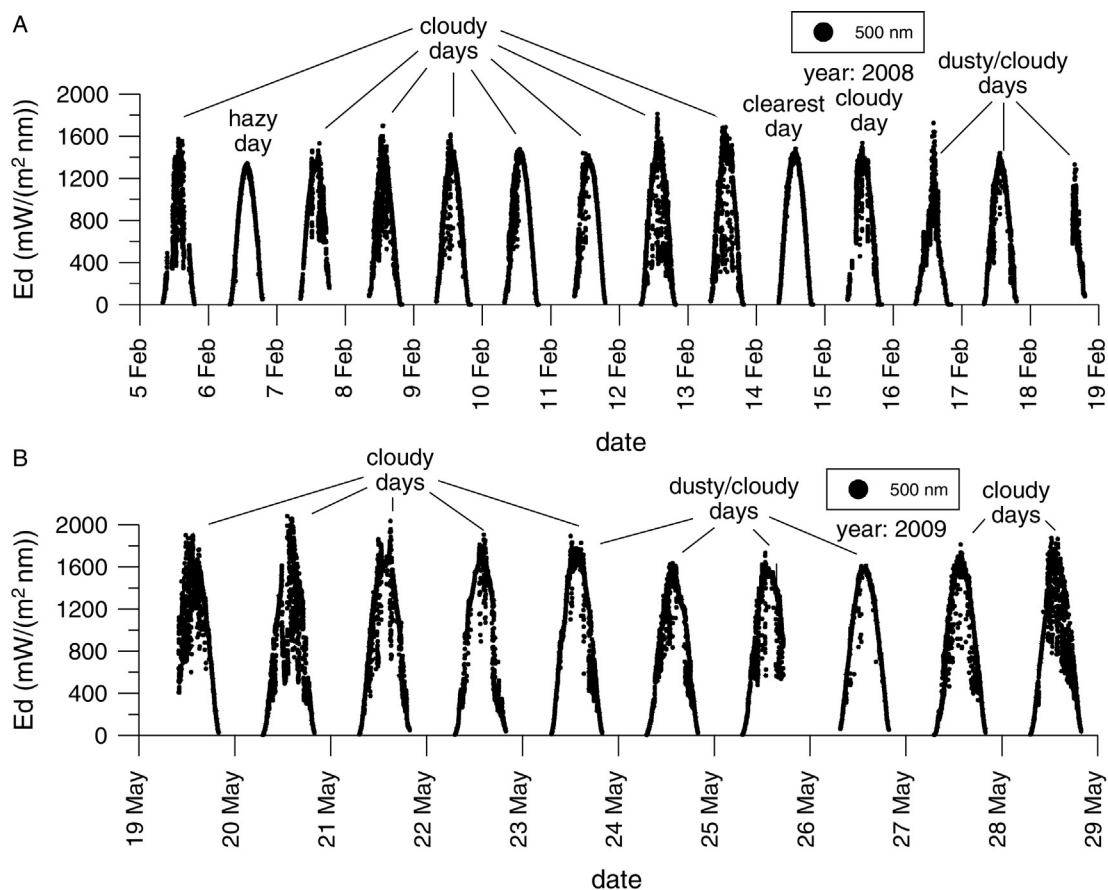


Fig. 3. The daily downward irradiances E_d at 500 nm measured during the two field campaigns are shown. 14 daily cycles were collected along the ship track (cf. with Fig. 1) in year 2008 (panel A). 10 daily cycles of downward irradiances were obtained at the permanent land station in Mindelo (cf. with Fig. 1) in the year 2009 (panel B). The downward irradiances were measured with a time resolution of 30 s. The observed daily irradiance cycles varied due to different atmospheric conditions. Clouds and dust events were indicated. The dust storms occurred between 16 and 19 February 2008 as well as between end of 23 and 27 May 2009. Outliers from the mean daily cycles represented the impact of clouds and dust on irradiance.

SAMUM-2 experiments in January and February 2008 (Knippertz et al., 2011, Weinzierl et al., 2011). For instance, pure dust and pure maritime layers in the lower atmosphere without biomass-burning layers aloft as well as maritime layers in the lower atmosphere with mixtures of dust and biomass-burning layers aloft were verified. Often mixtures of mostly dust and maritime particles below 1500 m and lofted layers of dust and smoke up to about 5000 m height were found (e.g. Knippertz et al., 2011; Tesche et al., 2011; Toledano et al., 2011). Our derived aerosol components could not be more accurately determined because of the lack of on-site measurements in our observation periods. But airborne and lidar measurements in the framework of SAMUM-2 delivered median AODs of 0.23 and 0.09 for dust and biomass-burning layers, respectively (Weinzierl et al., 2011). During both our field campaigns the strong dust storms on 16 February 2008 and 25 May 2009 caused

higher AOD_{dust} values. But the anthropogenic aerosol components with mean values between 0.04 and 0.05 were much smaller than 0.09 measured by Weinzierl et al. (2011). The mean values of 0.07–0.08 of maritime aerosol components were in the order of the average of 0.07 estimated in most ocean regions (Ramanathan et al., 2001; Smirnov et al., 2002).

3.2. Downward solar irradiance during cloudless, cloudy and dusty conditions

The downward solar irradiance at sea level of the two field campaigns in 2008 and 2009 is given in Fig. 3A and B.

The measured irradiances on 14 February 2008 were closest to the modelled cloud- and dust-free irradiances compared to all other observation days (see Fig. 4A and B). The dust AOD component of AOD was very low (see Fig. 2), and

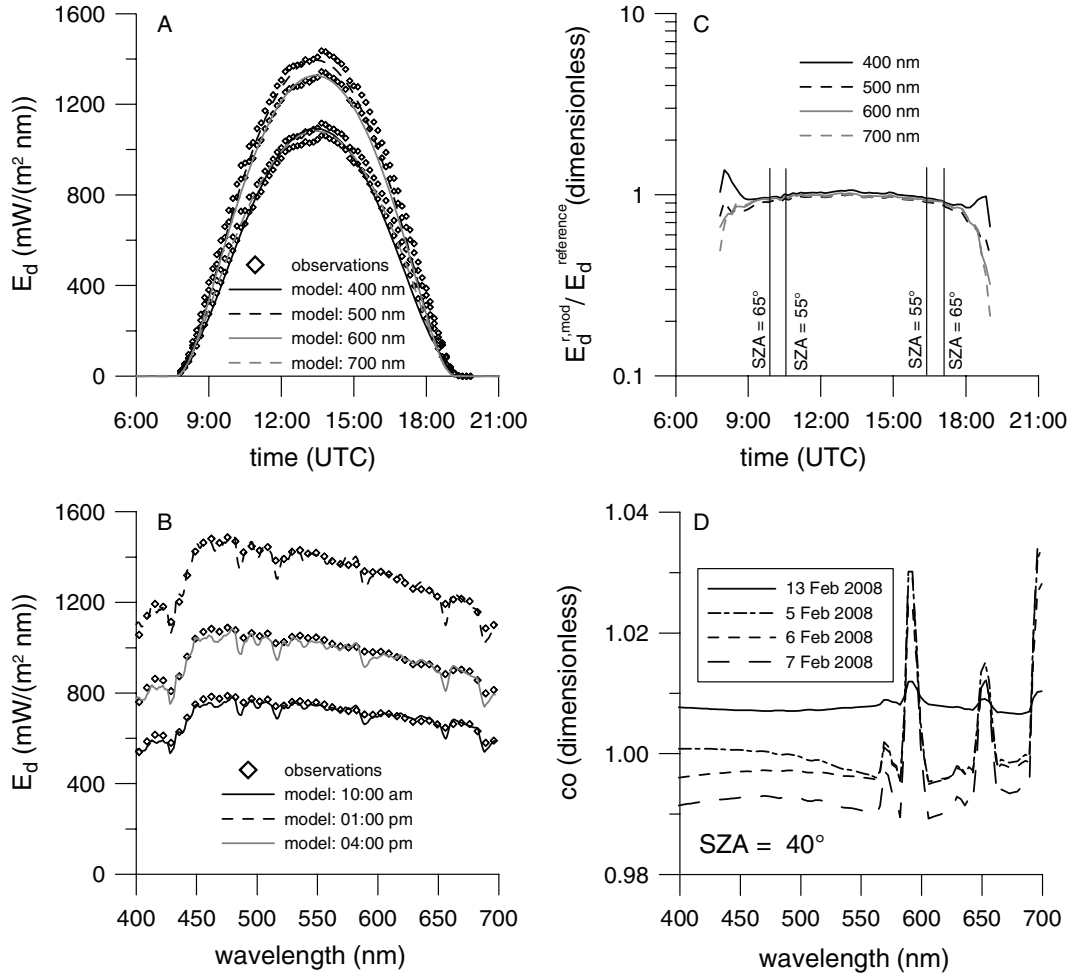


Fig. 4. Modelled downward irradiances $E_d^{r,mod}$ (Gregg and Carder, 1990) are compared with observations $E_d^{reference}$ on 14 February 2008 in dependence of time (panel A) and wavelength (panel B). The ratio between modelled irradiances $E_d^{r,mod}$ and measured irradiances $E_d^{reference}$ are shown for different wavelengths in Fig. 4C. The 14 February 2008 was the clearest day during both field campaigns. The observed irradiances matched very well the modelled ones because the spectral model was optimised for cloudless and dustless maritime atmospheres. The maximum differences were 5% for solar zenith angles (SZA) < 55 deg and higher than 10% for SZA > 65 deg. Correction terms (eq. 3) modelled on the basis of meteorological data set (see Sections 2.3.3 and 2.4.4) for different days are given in Fig. 4D (SZA = 40 deg). These terms were applied for the irradiance normalisation.

no cloud influence was observed in the irradiance measurements (see Fig. 3). The irradiance measurements on this day were used as reference irradiance $E_d^{reference}$ in Eqs. (1), (2) and (9). The diurnal variation of irradiance on 6 February 2008 was also well pronounced but was much lower because of the influence of haze. This day could not be used as reference.

Cloudy days were identified by comparison of observed irradiance to the reference irradiance (14 February 2008). Cloudy days were observed on 5, from 7 to 13 and from 15 to 19 February 2008 as well as between 19 and 29 May 2009. The irradiance measurements of the two different cases I and II were identified by their peaks. Irradiance peaks below the reference and modelled irradiances were

identified as clouds of case I and peaks above were considered as clouds of case II. These spectra were used as sample irradiances E_d^{sample} (*sample = cloud*) in Eqs. (1), (2) and (8).

The identified dusty days between 16 and 19 February 2008 and between 23 May and 27 May 2009 using the approach given in Section 3.1 were sporadically affected by clouds. But irradiances on 16 February 2008 were mainly influenced by clouds. Irradiance measurements during dusty atmospheric conditions without influence of clouds were selected and used as sample irradiances E_d^{sample} (*sample = dust*) in Eqs. (1), (2) and (8).

Please note that the sample irradiances of clouds and dust could be influenced by anthropogenic (biomass-burning

smoke) and maritime aerosols. The contribution of maritime aerosols could be neglected because of the generally much smaller absorption of sunlight compared to clouds, dust and biomass-burning smoke (e.g. Dubovik et al., 2002; Smirnov et al., 2002). But the light absorption in biomass-burning layers can be much stronger than in dust layers with 10 Mm^{-1} to 40 Mm^{-1} and 3 Mm^{-1} (Ansmann et al., 2011), respectively, which would have caused uncertainties in our results. The aerosol layer structures could not be resolved in detail during our observation periods because of the absence of certain on-site measurements. But the aerosol components were approximately determined by the separation approach of Kaufmann et al. (2005) (see Fig. 2). The aerosol ratios of $\text{AOD}_{\text{ma}}:\text{AOD}_{\text{an}}:\text{AOD}_{\text{dust}}$ given by 0.08:0.05:0.92 during the dust storm in February 2008 verified percentage ratios of 7.5%:4.8%:87.7%. It means that the light absorption in biomass-burning layers can be rather higher than in dust layers, but the contribution of biomass-burning aerosols to the total AOD can be much lower. However, the uncertainties increased for irradiance measurements at time periods besides dust storms if the different aerosol components were on a comparable level.

3.3. Correction term

The modelled and measured reference irradiances of 14 February 2008 were compared in Fig. 4A as a function of time for four different wavelengths and in Fig. 4B as a function of wavelength for three different times. Additionally, the ratio of modelled to measured irradiances is given in Fig. 4C. Fig. 4A–C approved the good correlation between both irradiances ($N=69$, $R^2=0.99$) with relative errors below 5% in the zenith range. The deviations were greater than 10% near the horizon. This verified the clear atmospheric conditions on 14 February 2008 and the usage of the corresponding irradiance observations as reference measurements $E_d^{\text{reference}}$ as well as of $E_d^{\text{r.mod}}$ as the modelled reference during clear atmospheric conditions.

The correction term (eq. 3) was calculated from the modelled clear sky reference $E_d^{\text{r.mod}}$ on 14 February 2008 and the modelled sample irradiance $E_d^{\text{s.mod}}$. The wavelength-dependent correction terms of different days are given in Fig. 4D for a fixed zenith angle of 40 deg. The correction terms varied around one in relation to the ratio of meteorological and atmospheric conditions during the days of modelled reference and sample irradiances. They were about one if the combination of these conditions produced similar modelled reference and sample irradiances. The maxima around 590 nm, 650 nm and 700 nm were induced by water vapour absorption bands, which cannot be resolved in the measurements.

3.4. Impact of clouds and Saharan dust on downward solar irradiance and photosynthetically available radiation

The maximum influence of clouds and Saharan dust on irradiance was determined by scanning of all derived relative irradiance deviations (eq. 2) of field campaigns 2008 and 2009. The procedure was restricted to zenith angles smaller than 60 deg because of the higher deviations of measured to modelled irradiances near the horizon. Their maximum spectral deviations were compared to irradiance during clear sky in Fig. 5.

The maximum reduction of downward solar irradiance by clouds of case I was between 58.9% and 67.2% at 400 nm and up to 84.4% at 700 nm (Table 1). These values corresponded to the results of Monteith (1973) and Kirk (1994). The total irradiance below a thin sheet of cirrus was reduced to 70% compared to clear sky and to 10% below a deep layer of stratus clouds (Monteith, 1973). Reductions between 50% and 80% were determined if clouds passed over the sun (Kirk, 1994). Frederick and Erlick (1997) revealed systematic wavelength dependence with reductions by clouds with up to 51% at 600 nm and up to 41% at 350 nm.

The spectral shape of the increase in the downward solar irradiance by clouds of case II was different from that of clouds of case I. The maximum enhancement was between 11.2% and 21.9% at 400 nm and between 24.9% and 34.0% at 700 nm in comparison to clear atmospheric conditions (Table 1). Kirk (1994) determined a smaller increase of total irradiance of 5–10% for a few isolated clouds in an otherwise clear sun and sky. The absolute modification of irradiance is of course much higher for clouds of case I than for clouds of case II because case I – clouds attenuated the direct and diffuse solar irradiance but case II – clouds increased the diffuse part.

The spectral dependence of relative irradiance deviation due to Saharan dust was different from that of clouds. Atmospheric dust reduced the incoming radiation especially in the blue spectral range. The reduction was between 9.3% and 19.7% at 400 nm for strong Saharan dust storms and between 1.0% and 4.1% at 700 nm (Table 1). The impact was in the short-wavelength range between 8.3% and 15.6% stronger than in the long-wavelength range.

During an aircraft experiment in Morocco, Otto et al. (2009) measured the downward irradiances below a dust plume on 19 May 2006. They derived a reduction of approximately 21% at 400 nm and 5% at 700 nm. Adeyefa et al. (1995) studied the spectral irradiance under Harmattan conditions, a dry and dusty West African trade wind blowing between November and March. They observed a severe reduction in the direct solar irradiance due to the strong attenuating effects of the Harmattan dust. During

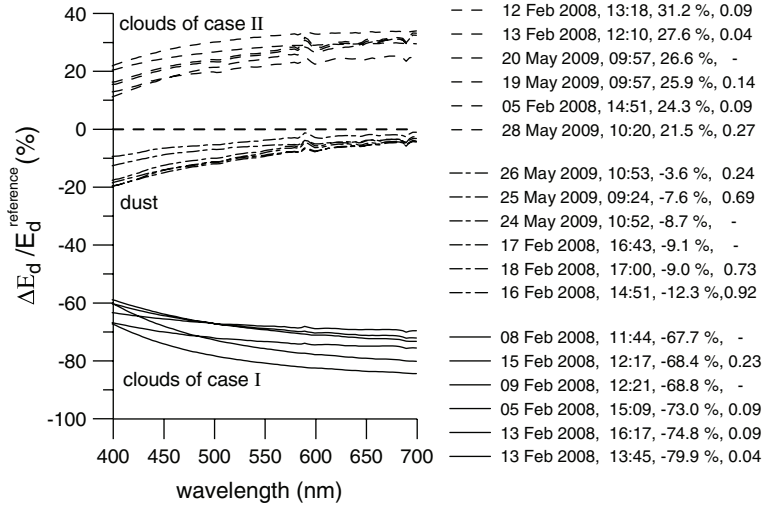


Fig. 5. The maximum relative irradiance deviations (eq. 2) due to case I – and case II – clouds as well as Saharan dust are shown. They were determined by scanning the whole data set of campaigns 2008 and 2009 with restriction to zenith angles smaller than 60 deg because of the higher deviations of measured to modelled irradiances near the horizon. The date and time of observation, the maximum relative deviation of photosynthetically available radiation (eq. 7) as well as the available dust components of aerosol optical depths of MODIS are shown on the right (see Section 2.4.2).

Saharan dust storms, Carlson and Caverly (1977) determined a decrease of about 20% of solar radiation in eastern equatorial Atlantic region, which is consistent with our findings.

The maximum relative deviation of photosynthetically available radiation (eq. 7) is given on the right-hand side of Fig. 5. Clouds of case I can considerably reduce Q_{PAR} up to 79.9% or up to about $1450 \mu\text{mol m}^{-2} \text{s}^{-1}$ in absolute values (cf. eq. 6). On the other hand, clouds of case II can enhance Q_{PAR} up to 31.2%, which corresponds to about $545 \mu\text{mol m}^{-2} \text{s}^{-1}$ (Table 1). The influence of Saharan dust storms on Q_{PAR} was smaller than that of clouds. The reduction was between 3.6% ($65 \mu\text{mol m}^{-2} \text{s}^{-1}$) and 12.3% ($210 \mu\text{mol m}^{-2} \text{s}^{-1}$) (Table 1).

The relative deviations of photosynthetically available radiation (eq. 7) of cloudy and dusty days in dependence of zenith angle are shown in Fig. 6. The 11 February 2008 was a cloudy day (black dots) and the 17 February was a dusty day with influence of clouds (dark grey dots). The dashed

line symbolised the case of a clear day. The highest and lowest values represented the maximum relative deviations of photosynthetically available radiation on these days in the zenith angle range between 30 and 60 deg.

The differences of both days depended on the zenith angle. The absolute values of the deviations increased with increasing zenith angles because the diffuse part of downward irradiance was increased. The relative deviations of Q_{PAR} were higher for the dusty day on 17 February 2008. The outliers on 11 and 17 February corresponded to the effect of clouds. Outliers above the daily mean were related to the impact of clouds of case II. Points below corresponded to the impact of clouds of case I. The influence of dust on the dependence of Q_{PAR} on zenith angle cannot be precisely determined from data set but it seems to be an enhancement of the effect with increasing zenith angles.

The modification of photosynthetically available radiation was compared with the dust component of the AOD of MODIS (AOD_{dust} in Section 2.4.2) in Fig. 7. The given

Table 1. Results of relative deviations of irradiance ($\Delta E_d / E_d^{\text{reference}}$) and photosynthetically available radiation ($\Delta Q_{PAR} / Q_{PAR}^{\text{reference}}$) are summarised. The maximum measured decrease (case I) and increase (case II) by clouds as well as the maximum decrease by dust are presented. (1) is the maximum measured decrease for the observed dust storms of both field campaigns, (2) is the decrease in dependence of dust component of aerosol optical depth (AOD) derived by a linear fit and (3) is the maximum decrease in the years 2008 and 2009 determined by the linear fit in combination with the maximum observed dust component of AOD in these years

	$\Delta E_d / E_d^{\text{reference}}$		$\Delta Q_{PAR} / Q_{PAR}^{\text{reference}}$
	400 nm	700 nm	400–700 nm
Cloud effect	–67.2% to +21.9%	–84.4% to +34.0%	–79.9% to +31.2%
Dust effect	–19.7%	–4.1%	(1): –12.3% (2): –1.2% per 0.1 AOD_{dust} (3): –31.9%

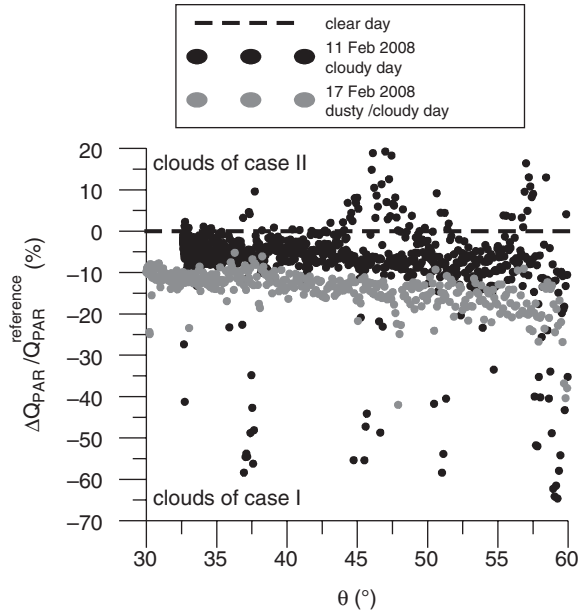


Fig. 6. The relative deviations of photosynthetically available radiation (eq. 7) of cloudy and dusty days are presented as a function of zenith angle. The deviations disappeared if the case of a clear day was assumed (dashed line). The outliers from the mean curves represented the impact of different cloud types.

points were separated into time-matched and not time-matched values by time difference between field and MODIS observations. Time-matched points are within a time difference less than 60 min. Fig. 7 implies that the photosynthetically available radiation decreased with increasing strength of Saharan dust storms. A linear fit was derived $\Delta Q_{\text{PAR}}/Q_{\text{PAR}}^{\text{reference}} = (-12.1 \pm 0.7) \cdot \text{AOD}_{\text{dust}}$ ($N = 13$, $R^2 = 0.95$, slope uncertainty = $0.7/12.1 \cdot 100\% = 5.8\%$) (Table 1). This fit was only valid for definite cases because the term $\Delta Q_{\text{PAR}}/Q_{\text{PAR}}^{\text{reference}}$ depended on the zenith angle (see Fig. 6) and AOD_{dust} depended on the wavelength used in the measurement of satellite AOD. Therefore, the fit was only significant for zenith angles between 35 and 50 deg and for AOD_{dust} values at wavelength of 550 nm. Furthermore, the relationship between $\Delta Q_{\text{PAR}}/Q_{\text{PAR}}^{\text{reference}}$ and AOD_{dust} was only derived from the two observed dust storms. The transport, profile, source of dust and therefore the dust optical properties could be varied in dependence of observation time. In the future, further irradiance measurements of various dust storms will show if the derived relationship is valid for different dust storms or is restricted to the observed dust storms in February 2008 and May 2009.

The combination of the dust storm statistics of Section 2.4.3 with the derived linear fit showed that photosynthetically available radiation was reduced at least by around 9% during strong Saharan dust storms, with AOD_{dust}

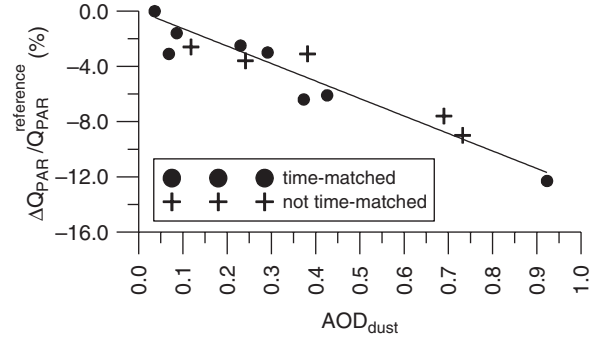


Fig. 7. The relative deviations of photosynthetically available radiation (eq. 7) are shown in dependence of dust component of the aerosol optical depth (AOD_{dust}). Points were classified to time-matched points if the time difference between field and MODIS observation was lower than 60 min. There are only few points in the figure because the AOD data of MODIS were limited by satellite swath and clouds.

values greater than 0.72. The linear relationship was also applied to all daily satellite-derived AOD_{dust} values (cf. Section 2.4.2) to determine the daily reduction of photosynthetically available radiation $|\Delta Q_{\text{PAR}}/Q_{\text{PAR}}^{\text{reference}}|$ for the years 2008 and 2009 (Fig. 8).

The time series of the reduction of photosynthetically available radiation in Fig. 8 reflects the sporadic Saharan dust events in winter and spring as well as the stronger and longer dust storms in summer and autumn. The occurrence of the summer and autumn dust events and the higher impact on photosynthetically available radiation can be explained by the migration of the intertropical convergence zone. This zone is part of the Hadley circulation cell and is responsible for the migration of maximum dust transport (e.g. Prospero and Carlson, 1972; Jankowiak and Tanré, 1992). The sporadic dust events and by that the sporadic reductions of photosynthetically available radiation in winter and spring were related to intense westward winds (e.g. Schepanski et al., 2009). In winter and spring, dust was spread over the ocean by spectacular dust storms in dust layers near the ocean surface. In summer and autumn, dust aerosols were transported between continental dry and marine wet trade winds in the upper atmosphere (e.g. Pérez-Marrero et al., 2002; Kaufman et al., 2005). Nevertheless, dust in both atmospheric layers reduced the photosynthetically available radiation in the study area on many days of 2008 and 2009 (see Fig. 8). A mean reduction of about 4.5% was determined. The reduction of photosynthetically available radiation was higher than the statistical limit of the sum of mean value and standard deviation (see upper dashed line of Fig. 8) for several dust storms in winter and spring but for many more events in summer and autumn. The highest dust component of AOD of 2.64 was determined on 17 July 2008. In the year 2009,

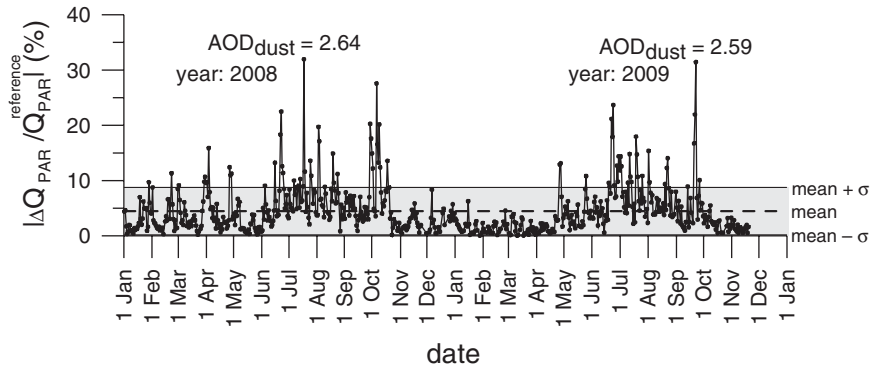


Fig. 8. The daily reductions of photosynthetically available radiation $|\Delta Q_{\text{PAR}}/Q_{\text{PAR}}^{\text{reference}}|$ by atmospheric dust are shown for the years 2008 and 2009. They were calculated on the basis of the linear fit (Section 3.4) and the dust components of aerosol optical depths (AODs) (cf. Section 2.4.2). The highest observed dust components of AODs of 2.64 on 17 July 2008 and of 2.59 on 22 September 2009 were marked. The corresponding highest reductions of photosynthetically available radiation were about 32% and 31%, respectively. The dashed line relates to the mean value of reduction. The shaded region corresponds to the standard deviation σ in the time period 2008 to 2009.

the highest value of 2.59 was derived on 22 September 2009. These major dust events decreased the photosynthetically available radiation by about 31.9% and 31.3% (Table 1), respectively.

4. Conclusions

The primary focus of the investigations was the impact of Saharan dust and clouds on photosynthetically available radiation in the area off NW Africa. Clouds reduced or enhanced the photosynthetically available radiation up to approximately 80% or 31%. The influence of atmospheric dust on photosynthetically available radiation of both observed dust storms was smaller than that of clouds. The reduction was between 4% and 12%, which corresponded to 6% and 15% of the cloud reduction. The derived reductions were only a snapshot of the situation in the study area. The decrease of photosynthetically available radiation should be certainly related to the temporal and spatial distribution of dust and clouds, and the ratio of clouds to dust cover should be considered in the future. The first step in this direction was taken because the main result of our investigations was the derivation of a relationship between the reduction of photosynthetically available radiation and the dust AOD. The relationship implies a decrease of nearly 1.2% in photosynthetically available radiation per increase of about 0.1 in the dust AOD. Based on this result a reduction in the photosynthetically available radiation of about 32% was derived for the strongest dust storm in July 2008 with a maximum dust AOD of 2.64. Another important result was the application of this relationship for the determination of the temporal development of photosynthetically available radiation due to Saharan dust between 2008 and 2009. The photosyntheti-

cally available radiation was often decreased in that time period, especially during sporadic winter and spring dust events and during the longer summer and autumn dust storms. Because of high frequency of dust storms in the area of NW Africa, the impact on photosynthetically available radiation should have a considerable influence on the ecosystem.

The dust storms do not only reduce the incoming solar radiation and photosynthetically available radiation. They modify the spectral composition of light due to the higher absorption in the blue spectral range, which should be important for photosynthetically active phytoplankton pigment and primary production, and should be investigated in the future.

5. Acknowledgements

The authors thank the Leibniz Institute for Baltic Sea Research for support and the German Federal Ministry of Education and Research (BMBF) for funding within the framework of the SOPRAN subproject: ‘Sahara dust impact on radiation transfer, optical properties and phytoplankton development in waters of the Cape Verde region’ (FKZ 03F0473E).

This research was based on MODIS aerosol data provided by NASA’s Giovanni, an online data visualisation and analysis tool (MODIS and SeaWiFS data) maintained by the Goddard Earth Sciences Data and Information Services Center, a section of the NASA Earth-Sun System Division (<http://giovanni.gsfc.nasa.gov>). QuikScat and AMSR-E data were produced by Remote Sensing Systems and sponsored by the NASA Ocean Vector Winds Science Team as well as by the NASA Earth Science DISCOVER Project. The data were available at <http://www.remss.com>. We thank the principal investigator D. Tanré for the

provision of AOD data of AERONET. NCEP reanalysis data were provided by the National Oceanic and Atmospheric Administration/Office of Oceanic and Atmospheric Research/Earth System Research Laboratory (NOAA/OAR/ESRL) Physical Science Division (PSD) from their Web site at <http://www.esrl.noaa.gov/psd/>. METAR – data were prepared by NCAR/EOL under sponsorship of the NSF (<http://data.eol.ucar.edu>). The MSG products were kindly provided by EUMETSAT.

We also thank anonymous reviewers for helpful comments on the manuscript.

References

- Adeyefa, Z. D., Holmgren, B. and Adedokun, J. A. 1995. Spectral solar irradiance under Harmattan conditions. *J. Renewable Energy*. **6**, 989–996.
- Alados, I., Olmo, F. J., Foyo-Moreno, I. and Alados-Arboledas, L. 2000. Estimation of photosynthetically active radiation under cloudy conditions. *Agric. For. Meteorol.* **102**, 39–50.
- Ansmann, A., Petzold, A., Kandler, K., Tegen, I., Wendisch, M. and co-authors. 2011. Saharan Mineral Dust Experiments SAMUM-1 and SAMUM-2: what have we learned? *Tellus B*. **63**(4), 403–429.
- Arnone, R. A. 1994. The temporal and spatial variability of chlorophyll in the western Mediterranean. In: *Seasonal and Interannual Variability of the Western Mediterranean Sea, Coastal Estuarine Studies* (ed. P. La Violette), Vol. 46, AGU, Washington, DC, pp. 195–225.
- Arnone, R. A., Ladner, S., La Violette, P. E., Brock, J. C. and Rochford, P. A. 1998. Seasonal and interannual variability of surface photosynthetically available radiation in the Arabian Sea. *J. Geophys. Res.* **103**(C4), 7735–7748.
- Barbosa, P. M., Stroppiana, D., Gregoire, J. M. and Pereira, J. M. C. 1999. An assessment of vegetation fire in Africa (1981–1991): burned areas, burned biomass, and atmospheric emissions. *Global Biogeochem. Cyc.* **13**, 933–950.
- Bartlett, J. S., Ciotti, Á. M., Davis, R. F. and Cullen, J. J. 1998. The spectral effects of clouds on solar irradiance. *J. Geophys. Res.* **103**(C13), 31017–31031. DOI:10.1029/1998JC900002.
- Bird, R. E. and Riordan, C. J. 1986. Simple solar spectral model for direct and diffuse irradiance on horizontal and tilted planes at the earth's surface for cloudless atmospheres. *J. Clim. Appl. Meteor.* **25**(1), 87–97.
- Bourassa, M. A., Legler, D., O'Brian, J. J. and Smith, S. R. 2003. SeaWinds validation with research vessels. *J. Geophys. Res.* **108**(C2), 3019. DOI:10.1029/2001JC001028.
- Carlson, T. N. and Caverly, R. S. 1977. Radiative characteristics of Saharan dust at solar wavelengths. *J. Geophys. Res.* **82**(21), 3141–3152. DOI:10.1029/JC082i021p03141.
- Carlson, T. N. and Benjamin, S. G. 1980. Radiative heating rates for Saharan dust. *J. Atmos. Sci.* **37**, 193–213.
- Chelton, D. B. and Freilich, M. H. 2005. Scatterometer-based assessment of 10 m wind analysis from the operational ECMWF and NCEP numerical weather prediction models. *Mon. Wea. Rev.* **133**, 409–429.
- Chen, G., Ziemba, L. D., Chu, D. A., Thornhill, K. L., Schuster, G. L. and co-authors. 2010. Observation of Saharan dust microphysical and optical properties from the Eastern Atlantic during NAMMA airborne field campaign. *Atmos. Chem. Phys. Discuss.* **11**, 723–740.
- Chiapello, I. and Moulin, C. 2002. TOMS and METEOSAT satellite records of the variability of Saharan dust transport over the Atlantic during the last two decades (1979–1997). *Geophys. Res. Lett.* **29**(8), 1176. DOI:10.1029/2001GL013767.
- Claustre, H., Morel, A., Hooker, S. B., Babin, M., Antoine, D. and co-authors. 2002. Is desert dust making oligotrophic waters greener? *Geophys. Res. Lett.*, **29**(10), 1469. DOI:10.1029/2001GL014056.
- Davies, J. A. 1995. Comparison of modeled and observed global irradiance. *J. Appl. Meteorol.* **35**, 192–201.
- Dickey, T. and Simpson, J. J. 1983. The influence of optical water type on the diurnal response of the upper ocean. *Tellus B*. **35**, 142–154.
- Drouin, A. and Karcher, F. 2004. High resolution ozone column derived from SEVIRI 9.7 ozone channel. In: *Proceedings Second MSG RAO Workshop*, Salzburg, Austria, 9–10 September 2004 (ESA SP-582, November 2004).
- Dubovik, O., Holben, B., Eck, T. F., Smirnov, A., Kaufman, Y. J. and co-authors. 2002. Variability of absorption and optical properties of key aerosol types observed in worldwide locations. *J. Atmos. Sci.* **59**, 590–608.
- Ebuchi, N., Graber, H. C. and Caruso, M. J. 2002. Evaluation of wind vectors observed by QuikSCAT/SeaWinds using ocean buoy data. *Am. Meteorol. Soc.* **19**, 2049–2062.
- Ebuchi, N. 2006. Evaluation of marine surface winds observed by SeaWinds and AMSR on ADEOSII. *J. Oceanogr.* **62**, 293–301.
- Frederick, J. E. and Erlick, C. 1997. The attenuation of sunlight by high-latitude clouds: spectral dependence and its physical mechanisms. *J. Atmos. Sci.* **54**, 2813–2819.
- Frouin, R. and Murakami, H. 2007. Estimating photosynthetically available radiation at the ocean surface from ADEOS-II global imager data. *J. Oceanogr.* **22**(3), 493–503. DOI: 10.1007/s10872-007-0044-3.
- Gordon, H. R., Clark, D. K., Brown, J. W., Brown, O. W., Evans, R. H. and co-authors. 1983. Phytoplankton pigment concentrations in the Middle Atlantic Bight: comparison of ship determinations and CZCS estimates. *Appl. Optics.* **22**(1), 20–36. DOI:10.1364/AO.22.000020.
- Goudie, A. S. and Middleton, N. J. 2001. Saharan dust storms: nature and consequences. *Earth Sci. Rev.* **56**, 179–204.
- Gregg, W. W. and Carder, K. L. 1990. A simple spectral solar irradiance model for cloudless maritime atmospheres. *Limnol. Oceanogr.* **35**, 1657–1675.
- Haywood, J., Francis, P., Osborne, S., Glew, M., Loeb, N. and co-authors. 2003. Radiative properties and direct radiative effect of Saharan dust measured by the C-130 aircraft during SHADE: 1. Solar spectrum. *J. Geophys. Res.* **108**(D18), 8577. DOI:10.1029/2002JD002687.
- Haywood, J. M., Pelon, J., Formenti, P., Bharmal, N., Brooks, M. and co-authors. 2008. Overview of the dust and biomass-burning experiment and African Monsoon multidisciplinary

- analysis special observing period-0. *J. Geophys. Res.* **113**(D00C17). DOI:10.1029/2008JD010077.
- Heuermann, R., Reuter, R. and Willkomm, R. 1999. RAMSES: a modular multispectral radiometer for light measurements in the UV and VIS. *Environ. Sens. Appl. Proc. EUROPTO Series. SPIE.* **3821**, 279–285.
- Holben, B. N., Eck, T. F., Slutsker, I., Tanré, D., Buis, J. P. and co-authors. 1998. AERONET – a federated instrument network and data archive for aerosol characterization. *Rem. Sens. Environ.* **66**, 1–16.
- Jankowiak, I. and Tanré, D. 1992. Satellite climatology of Saharan dust outbreaks. *J. Clim.* **5**, 646–656.
- Jerlov, N. G. 1976. *Marine Optics*. Amsterdam, Elsevier.
- Jimin, Y., Xiaoqing, G., Qi, F., Xiaoyou, Z. and Lianglei, G. 2006. The photosynthetically active radiation during dust storm day in Ejina Oasis. *Acta Energiæ Solaris Sinica*, **5**, 488–494.
- Kalnay, E., Kanamitsu, M., Kistler, R., Collins, W., Deaven, D. and co-authors. 1996. The NCEP/NCAR 40-Year Reanalysis Project. *Bull. Am. Meteorol. Soc.* **77**, 437–470.
- Kalu, A. E. 1979. The African Dust Plume: its characteristics and propagation across West Africa in winter. In: *Saharan Dust. Mobilization, Transport, Deposition* (ed. C. Morales (Hg.)) *Papers and Recommendations from a Workshop held in Gothenburg, Sweden, 25–28 April 1977*, Chichester, New York, Brisbane, Toronto, pp. 95–118.
- Kanamitsu, M., Ebisuzaki, W., Woollen, J., Yang, S. K., Hnilo, J. J. and co-authors. 2002. NCEP-DEO AMIP-II reanalysis (R-2). *Bull. Am. Meteorol. Soc.* **83**, 1631–1643.
- Kasten, F. and Czeplak, G. 1980. Solar and terrestrial radiation dependent on the amount and type of cloud. *Sol. Energy.* **24**, 177–189.
- Kaufman, Y. J., Koren, I., Remer, L. A., Tanré, D., Ginoux, P. and co-authors. 2005. Dust transport and deposition observed from the Terra-Moderate Resolution Imaging Spectroradiometer (MODIS) spacecraft over the Atlantic Ocean. *J. Geophys. Res.* **110**, D10S12. DOI:10.1029/2003JD004436.
- Kirk, J. T. O. 1977. Use of a quanta meter to measure attenuation and underwater reflectance of photosynthetically active radiation in some inland and coastal south-east Australian waters. *Aust. J. Mar. Freshwater Res.* **28**, 9–21.
- Kirk, J. T. O. 1994. *Light and Photosynthesis in Aquatic Ecosystems*. Cambridge University Press, Cambridge, United Kingdom.
- Knippertz, P., Tesche, M., Heinold, B., Kandler, K., Toledano, C. and co-authors. 2011. Dust mobilization and aerosol transport from West Africa to Cape Verde – a meteorological overview of SAMUM-2. *Tellus B.* **63**(4), 430–477.
- Lieke, K., Kandler, K., Scheuven, C., Emmel, C., von Glahn, C. and co-authors. 2011. Particle chemical properties in the vertical column based on aircraft observations in the vicinity of Cape Verde Islands. *Tellus B.* **63**(4), 497–511.
- Mallet, M., Chami, M., Gentili, B., Sempéré, R. and Dubuisson, P. 2009. Impact of sea-surface dust radiative forcing on the oceanic primary production: a 1D modeling approach applied to the West African coastal waters. *Geophys. Res. Lett.* **36**, L15828. DOI:10.1029/2009GL039053.
- Monteith, J. L. 1973. *Principles of Environmental Physics*. Edward Arnold, London.
- Morel, A. and Smith, R. C. 1982. Terminology and units in optical oceanography. *Mar. Geod.* **5**(4), 335–349. DOI: 10.1080/15210608209379431.
- Otto, S., Bierwirth, E., Weinzierl, B., Kandler, K., Esselborn, M. and co-authors. 2009. Solar radiative effects of a Saharan dust plume observed during SAMUM assuming spheroidal model particles. *Tellus B.* **61**, 270–296. DOI: 10.1111/j.1600-0889.2008.00389.x.
- Pérez-Marrero, J., Llinas, O., Maroto, L., Rueda, M. J. and Cianca, A. 2002. Saharan dust storms over the The Canary Islands during winter 1998 as depicted from the advanced very high-resolution radiometer. *Deep-Sea Res. II.* **49**, 3465–3479.
- Petzold, A., Veira, A., Mund, M., Esselborn, C., Kiemle, B. and co-authors. 2011. Mixing of mineral dust with urban pollution aerosol over Dakar (Senegal): impact on dust physico-chemical and radiative properties. *Tellus B.* **63**(4), 619–634.
- Prospero, J. M. and Carlson, T. N. 1972. Vertical and areal distribution of Saharan dust over the Western Equatorial North Atlantic Ocean. *J. Geophys. Res.* **77**, 5255–5265.
- Prospero, J. M., Glaccum, R. A. and Nees, R. T. 1981. Atmospheric transport of soil dust from Africa to South America. *Nature.* **289**, 570–572.
- Prospero, J. M. and Lamb, P. J. 2003. African droughts and dust transport to the 638 Caribbean: climate change implications. *Science.* **302**, 1024–1027.
- Ramanathan, V., Crutzen, P. J., Lelieveld, J., Mitra, A. P., Althausen, D. and co-authors. 2001. The Indian Ocean Experiment: an integrated analysis of the climate forcing and effects of the great Indo-Asian haze. *J. Geophys. Res.* **106**, 28371–28398.
- Remer, L. A., Tanré, D., Kaufman, Y. J., Ichoku, C., Mattoo, S. and co-authors. 2002. Validation of MODIS aerosol retrieval over ocean. *Geophys. Res. Lett.* **29**(12), 8008.
- Schepanski, K., Tegen, I. and Macke, A. 2009. Saharan dust transport and deposition towards the tropical northern Atlantic. *Atmos. Chem. Phys.* **9**, 1173–1189.
- Seckmeyer, G., Bais, A., Bernhard, G., Blumthaler, M., Booth, C. R. and co-authors. 2005. Instruments to Measure Solar Ultraviolet Radiation Part 2: Broadband Instruments Measuring Erythemally Weighted Solar Irradiance, WMO GAW Report No. 164, Geneva.
- Smirnov, A., Holben, B. N., Kaufman, Y. J., Dubovik, O., Eck, T. F. and co-authors. 2002. Optical properties of atmospheric aerosol in maritime environments. *J. Atmos. Sci.* **59**, 501–523.
- Stephens, G. L. and Tsay, S-C. 1990. On the cloud absorption anomaly. *QJR Meteorol. Soc.* **116**, 671–704.
- Stramska, M., Stramski, D., Cichocka, M., Cieplak, A. and Wozniak, S. B. 2008. Effects of atmospheric particles from Southern California on the optical properties of seawater. *J. Geophys. Res.* **113**, C08037. DOI:10.1029/2007JC004407.
- Tanré, D., Herman, M. and Kaufman, Y. J. 1996. Information on aerosol size distribution contained in solar reflected radiances. *J. Geophys. Res.* **101**, 19043–19060.
- Tanré, D., Kaufman, Y. J., Herman, M. and Mattoo, S. 1997. Remote sensing of aerosol over oceans from EOS-MODIS. *J. Geophys. Res.* **102**, 16971–16988.
- Tanré, D., Haywood, J., Pelon, J., Léon, J. F. and Chatenet, B. 2003. Measurement and modeling of the Saharan dust radiative

- impact: overview of the Saharan Dust Experiment (SHADE). *J. Geophys. Res.* **108**(D18), 8574. DOI:10.1029/2002JD003273.
- Tesche, M., Müller, D., Gross, S., Ansmann, A., Althausen, D. and co-authors. 2011. Optical and microphysical properties of smoke over Cape Verde inferred from multiwavelength lidar measurements. *Tellus B.* **63**(4), 677–694.
- Toledano, C., Wiegner, M., Groß, S., Freudenthaler, V., Gasteiger, J. and co-authors. 2011. Optical properties of aerosol mixtures derived from sun-sky radiometry during SAMUM-2. *Tellus B.* **63**(4), 635–648.
- Udo, S. O. and Aro, T. O. 1999. Global PAR related to global solar radiation for central Nigeria. *Agric. For. Meteorol.* **97**, 21–31.
- Weinzierl, B., Sauer, D., Esselborn, M., Petzold, A., Veira, A. and co-authors. 2011. Microphysical and optical properties of dust and tropical biomass burning aerosol layers in the Cape Verde region – an overview of the airborne in situ and lidar measurements during SAMUM-2. *Tellus B.* **63**(4), 589–618.
- Willson, R. C. and Mordvinov, A. V. 2003. Secular total solar irradiance trend during solar cycles 21–23. *Geophys. Res. Lett.* **30**(5), 1199. DOI:10.1029/2002GL016038.
- Wiggert, J. D. and Murtugudde, R. G. 2007. The sensitivity of the Southwest Monsoon phytoplankton bloom to variations in aeolian iron deposition over the Arabian Sea. *J. Geophys. Res.* **112**, c05005. DOI:10.1029/2006JC003514.
- Wozniak, S. B. and Stramski, D. 2004. Modeling the optical properties of mineral particles suspended in seawater and their influence on ocean reflectance and chlorophyll estimation from remote sensing algorithms. *Appl. Opt.* **43**(17), 3489–3503.
- Wuttke, S., Naggar, S. E., Bluszcz, T. and Schrems, O. 2007. Shipborne measurements of erythemal UV irradiance and ozone content in various climate zones. *Photochem. Photobiol. Sci.* **6**, 1081–1088.